

UNIVERSITY OF CALIFORNIA

Los Angeles

Some Adventures in
Secondary Ammonium Ion
Binding

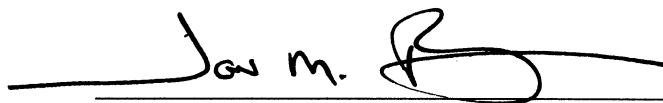
A dissertation submitted in partial satisfaction of the
requirements for the degree Doctor of Philosophy
in Chemistry

by

Stuart James Cantrill

2001

The dissertation of Stuart James Cantrill is approved.

A handwritten signature in black ink, appearing to read "Jon M. Fukuto", written over a horizontal line.

Jon M Fukuto

A handwritten signature in black ink, appearing to read "Miguel A Garcia-Garibay", written over a horizontal line.

Miguel A Garcia-Garibay

A handwritten signature in black ink, appearing to read "James Fraser Stoddart", written over a horizontal line.

J Fraser Stoddart, Committee Chair

University of California, Los Angeles

2001

For my parents

Pamela and Barrie

and

for my wife

Maggie

TABLE OF CONTENTS

Chapter 1: A Molecular Meccano Kit	1
Table of Contents	2
1.0. Abstract	3
1.1. Introduction	3
1.2. In the Beginning	5
1.3. Multiply Encircled Complexes	8
1.4. Controlling the Extended Superstructure	11
1.5. Changing the Rings and Ringing the Changes	19
1.5.1. <i>Tetrabenzo[24]crown-8 (TB24C8)</i>	20
1.5.2. <i>Benzometaphenylene[25]crown-8 (BMP25C8)</i>	23
1.5.3. <i>Tribenzo[27]crown-9 (TB27C9)</i>	25
1.5.4. <i>Bisparaphenylene[34]crown-10 (BPP34C10)</i>	27
1.6. Supramolecular Bundles	29
1.7. Mixing and Matching	33
1.8. How Large can these Superstructures be?	37
1.9. Conclusions	39
1.10. References and Notes	40
Chapter 2: The Influence of Macrocyclic Polyether Constitution upon Ammonium Ion Binding	48
Table of Contents	49
2.0. Abstract	50
2.1. Introduction	50
2.2. Synthesis	51
2.3. Mass Spectrometric Studies	53
2.4. Solution Phase Studies	54
2.4.1. <i>[24]Crown-8-Based Macrocycles</i>	55
2.4.2. <i>[25]Crown-8-Based Macrocycles</i>	57
2.4.3. <i>Summary of Solution Phase Studies</i>	59
2.5. X-Ray Crystallographic Investigations	60
2.5.1. <i>Background</i>	60
2.5.2. <i>Tetrabenzo[24]crown-8 (TB24C8)</i>	61
2.5.3. <i>Benzometaphenylene[25]crown-8 (BMP25C8)</i>	67
2.6. Conclusions	69
2.7. Experimental	71
2.8. References and Notes	76

Chapter 3: Supramolecular Daisy Chains	84
Table of Contents	85
3.0. Abstract	86
3.1. Introduction	86
3.2. [24]Crown-8-Based Systems	91
3.2.1. <i>The Parent Monomer</i>	91
3.2.2. <i>A Deuterated Monomer</i>	107
3.2.3. <i>Two Fluorinated Monomers</i>	110
3.3. [25]Crown-8-Based Systems	126
3.3.1. <i>The Parent Monomer</i>	127
3.3.2. <i>A Fluorinated Monomer</i>	129
3.4. Conclusions	137
3.5. Future Directions	138
3.6. Experimental	140
3.7. References and Notes	153
Chapter 4: Kinetic and Thermodynamic Approaches for the Synthesis of Ammonium Ion/Crown Ether-Based Interlocked Molecules	163
Table of Contents	164
4.0. Abstract	165
4.1. Introduction	165
4.1.1. <i>Threading, Clipping, and Slipping: How to Make Interlocked Molecules</i>	166
4.1.2. <i>Kinetic and Thermodynamic Considerations</i>	169
4.2. A Kinetic Approach – Urea Formation	172
4.2.1. <i>A DB24C8-Containing [2]Rotaxane</i>	173
4.2.2. <i>A BMP25C8-Containing [2]Rotaxane</i>	178
4.3. A Thermodynamic Approach – Imine Formation	185
4.3.1. <i>A Dynamic [2]Rotaxane</i>	185
4.3.2. <i>Future Outlook: Imine Exchange</i>	191
4.4. Conclusions	193
4.5. Experimental	194
4.6. References and Notes	200
Appendix	208

LIST OF FIGURES

Chapter 1: A Molecular Meccano Kit

- Figure 1.1.** A schematic representation depicting the formation of a threaded 1:1 complex (a [2]pseudorotaxane) between two complementary species wherein the cavity of a suitably-sized macrocycle is pierced by a linear thread. 6
- Figure 1.2.** One of the two distinct superstructures adopted in the solid state by the [2]pseudorotaxane [DB24C8·DBA]⁺. 7
- Figure 1.3.** π - π Stacking of the benzyl rings of the [2]pseudorotaxane [DB24C8·DBA]⁺ produces an infinite linear pseudopolyrotaxane. 7
- Figure 1.4.** The solid-state superstructure of a [3]pseudorotaxane [(DB24C8)₂·1]²⁺ formed between a thread-like molecule—containing *two* ammonium centers (1·2PF₆)—and *two* DB24C8 macrocycles. 9
- Figure 1.5.** The solid-state superstructure of a [4]pseudorotaxane [(DB24C8)₃·2]³⁺ formed between a thread-like molecule—containing *three* ammonium centers (2·3PF₆)—and *three* DB24C8 macrocycles. 9
- Figure 1.6.** The influence of both directionality and steric crowding upon solid-state superstructures assembled *via* the carboxylic acid dimer are highlighted. The *para* disposition of carboxylic acid groups in terephthalic acid (**a**) results in the formation of infinite linear tapes, whereas the *meta* disposition—as in isophthalic acid (**b**)—produces a crinkled tape. The sterically congested 5-decyloxyisophthalic acid (**c**) is precluded from forming an extended tape superstructure, assembling instead into discrete hexameric supramacrocycles. 11
- Figure 1.7.** The solid-state superstructure of the [2]pseudorotaxane [DB24C8·4]⁺ formed between the *para*-carboxylic acid-substituted DBA⁺ cation 4⁺ and DB24C8. 13
- Figure 1.8.** An infinite linear daisy-chain-like array of [DB24C8·4]⁺ is formed as a result of hydrogen bonding between the carboxylic acid of one thread and the crown ether component of a neighboring [2]pseudorotaxane. 14
- Figure 1.9.** The solid-state superstructure of the [2]pseudorotaxane [DB24C8·5]⁺ formed between the bis-*para*-carboxylic acid-substituted DBA⁺ cation 5⁺ and DB24C8. 15
- Figure 1.10.** Despite the formation of a carboxylic acid dimer between individual [2]pseudorotaxanes, the possibility of an infinite hydrogen bonded polymer is negated by the formation of hydrogen bonds from the terminal carboxylic acid protons to included acetone molecules in the solid-state superstructure of [DB24C8·5]⁺. 15
- Figure 1.11.** The solid-state superstructure of the [2]pseudorotaxane [DB24C8·6]⁺ formed between the bis-*meta*-carboxylic acid-substituted DBA⁺ cation 6⁺ and DB24C8. 16
- Figure 1.12.** The X-ray crystallographic analysis of [DB24C8·6][PF₆] reveals the formation—in the solid state—of a carboxyl-dimer-linked main chain pseudopolyrotaxane. 17

Figure 1.13. The solid-state superstructure of the [2]pseudorotaxane [DB24C8·7] ⁺ formed between the isophthalic acid-substituted DBA ⁺ cation 7 ⁺ and DB24C8.	18
Figure 1.14. The side-chain pseudopolyrotaxane formed as a result of carboxylic acid dimerization in the extended superstructure of [DB24C8·7] ⁺ .	19
Figure 1.15. When grown from a MeCN/Et ₂ O solution, crystals of TB24C8 can be seen to contain enclathrated acetonitrile molecules.	21
Figure 1.16. In the absence of MeCN, TB24C8 crystallizes without ordered solvent molecules.	22
Figure 1.17. One of the four crystallographically independent superstructures with a [2]pseudorotaxane geometry observed in the X-ray analysis of [TB24C8·DBA][PF ₆].	22
Figure 1.18. The extensively C–H···F hydrogen bond-stabilized extended superstructure of the complex [TB24C8·DBA][PF ₆].	22
Figure 1.19. The solid-state superstructure of the [2]pseudorotaxane [BMP25C8·DBA] ⁺ formed between the DBA ⁺ cation and BMP25C8.	24
Figure 1.20. Discrete [BMP25C8·DBA] ⁺ supermolecules are linked in the solid state to form extended sheets.	24
Figure 1.21. The solid-state structure of BMP25C8.	25
Figure 1.22. Constricted nanotubes—stabilized by intermolecular C–H···O hydrogen bonds—are formed by the stacking of BMP25C8 molecules in the solid state.	25
Figure 1.23. The solid-state superstructure of the [2]pseudorotaxane [TB27C9·(<i>p</i> -CO ₂ Me) ₂ -DBA] ⁺ formed between the <i>p</i> -CO ₂ Me-disubstituted DBA ⁺ cation and TB27C9.	26
Figure 1.24. The extended superstructure of [TB27C9·(<i>p</i> -CO ₂ Me) ₂ -DBA][PF ₆] consists of extended sheets that are stabilized by inter-[2]pseudorotaxane C–H···π hydrogen bonds.	26
Figure 1.25. The solid-state superstructure of a <i>double-stranded</i> [3]pseudorotaxane [BPP34C10·(DBA) ₂] ²⁺ formed between BPP34C10 and DBA·PF ₆ .	27
Figure 1.26. Conceivably, there are four possible distinct superstructures that may form upon co-crystallization of BPP34C10 and 1·2PF ₆ : (a) a <i>single-threaded, double-docked</i> [2]pseudorotaxane, (b) a <i>double-threaded, double-encircled</i> [4]pseudorotaxane, (c) a face-to-face complex, and (d) a polymer.	28
Figure 1.27. The solid-state superstructure of the <i>double-threaded, double-encircled</i> [4]pseudorotaxane [(BPP34-C10) ₂ ·(1) ₂] ⁴⁺ formed between BPP34C10 and 1 ²⁺ .	28
Figure 1.28. Individual [2 + 2] superbundles form columns in the solid state. The interstitial PF ₆ [−] anions may play some role in the assembly of this infinite one-dimensional array.	29
Figure 1.29. The solid-state superstructure of the five-component superbundle [(BPP34C10) ₃ ·(8) ₂] ⁶⁺ formed between the trifurcated tris-ammonium cation 8 ³⁺ and the ditopic crown ether BPP34C10.	30
Figure 1.30. Interleaved one-dimensional arrays of the five-component superbundle [(BPP34C10) ₃ ·(8) ₂] ⁶⁺ are formed in the solid state.	31

- Figure 1.31.** Co-crystallization of BPP34C10 and **9**·PF₆ affords a six-component superbundle that is a supramolecular analogue of the photosynthetic special pair. 32
- Figure 1.32.** The solid-state superstructure of a *triple-threaded* 1:1 complex formed between a trifurcated trisammonium thread and a complementary triphenylene-based tris-DB24C8 derivative. 33
- Figure 1.33.** In a manner analogous to DBA·PF₆, **4**·PF₆ forms a *double-threaded* [3]pseudorotaxane when co-crystallized with BPP34C10. 34
- Figure 1.34.** Individual [BPP34C10·(**4**)₂][2PF₆] [3]pseudorotaxanes dimerize in the solid state *via* the formation of carboxylic acid dimers. 35
- Figure 1.35.** Similarly to **4**·PF₆, its *meta*-substituted cousin **10**·PF₆ forms a 1:2 complex when co-crystallized with BPP34C10. 35
- Figure 1.36.** Discrete [BPP34C10·(**10**)₂][2PF₆] supermolecules dimerize—in the solid state—as a result of carboxyl dimer formation. 36
- Figure 1.37.** Two 7⁺ cations thread through the cavity of BPP34C10 in a centrosymmetric fashion, resulting in the formation of a [3]pseudorotaxane [BPP34C10·(**7**)₂]²⁺ in the solid state. 36
- Figure 1.38.** Analysis of the extended solid-state superstructure adopted by [BPP34C10·(**7**)₂]²⁺ reveals the existence of an interwoven cross-linked supramolecular polymer. 37
- Figure 1.39.** The extended crown ether TPP51C15 co-crystallizes with *three* equivalents of DBA·PF₆ to give a *triple-threaded* [4]pseudorotaxane [TPP51C15·(DBA)₃]³⁺. Note how a PF₆⁻ anion occupies a cleft in the superstructure. 38
- Figure 1.40.** The extended crown ether TPP68C20 co-crystallizes with *four* equivalents of DBA·PF₆ to give a *quadruple-threaded* [5]pseudorotaxane [TPP68C20·(DBA)₄]⁴⁺. One PF₆⁻ anion is encapsulated completely within the superstructure. 39

Chapter 2: The Influence of Macrocyclic Polyether Constitution upon Ammonium Ion Binding

- Figure 2.1.** The *face-to-face* interaction between DB18C6 and a primary ammonium ion. 50
- Figure 2.2.** Top: A schematic representation depicting the formation of a threaded 1:1 complex (a *Pseudorotaxane*) formed between two complementary species, whereupon the cavity of a suitably-sized *Ring*-shaped component is skewered by a linear *Thread*-like one. Bottom: A specific example of this concept showing how the dibenzylammonium cation 7⁺ threads through DB24C8 (**3**). 51
- Figure 2.3.** The LSI-mass spectrum of a 1:1 mixture of DB24C8 (**3**) and **9**·PF₆. 54
- Figure 2.4.** Partial ¹H NMR spectrum (400 MHz, CD₃CN, 300 K), of an equimolar solution of DB24C8 (**3**) and **9**·PF₆ (both 10 mM), demonstrating that complexed (c) and uncomplexed (uc) species are equilibrating with one another slowly on the ¹H NMR timescale. 56

- Figure 2.5.** Partial ^1H NMR spectra (the AA'BB' region) of a 1:1 mixture of BMP25C8 (**5**) and **9**-PF₆ in CD₃CN solution over the temperature range 243-300 K. 58
- Figure 2.6.** The van't Hoff plot obtained upon plotting $\ln K_a$ vs $1/T$ for the K_a values determined—using the single point method—over the temperature range 243-288 K. 59
- Figure 2.7.** The X-ray crystal superstructure of [3·7]PF₆. 60
- Figure 2.8.** Ball-and-stick representations of the four crystallographically-independent [2]pseudorotaxanes present in the crystals of [4·7]PF₆ showing the N⁺-H···O and C-H···O hydrogen bonding. The hydrogen bonding geometries and inter-ring separations are given in Table 2.3. 61
- Figure 2.9.** (a) Ball-and-stick and (b) space-filling representations (hydrogen atoms omitted for clarity) showing the layer structure of [4·7]PF₆. 63
- Figure 2.10.** A space-filling representation (hydrogen atoms omitted for clarity) of [4·7]PF₆ showing the embedding of the PF₆⁻ anions into the egg-box-like clefts formed in the layer structure of [2]pseudorotaxane supermolecules. 64
- Figure 2.11.** The solid-state superstructure of TB24C8·2MeCN. 64
- Figure 2.12.** The C-H···π-linked supramolecular chain formed by TB24C8·2MeCN in the solid state. 65
- Figure 2.13.** The solid-state structure of TB24C8. 65
- Figure 2.14.** (a) Part of one of the C-H···π (aryl-methine) linked sheets of molecules present in the solid-state superstructure of TB24C8, and (b) the linking of the adjacent sheets by means of C-H···π (*O*-methylene) interactions. 66
- Figure 2.15.** The systematic approaches of the aryl-methine and *O*-methylene protons to the opposite faces of all four catechol rings (A, A', B and B') in the solid-state superstructure of TB24C8. 67
- Figure 2.16.** The X-ray crystal superstructure of the [2]pseudorotaxane [5·7-H]⁺ formed between BMP25C8 (**5**) and the dibenzylammonium cation 7⁺. Hydrogen bonding distances and angles {[N⁺···O], [H···O] distances (Å), [N-H···O] angles (°)}: (a) 2.91, 2.06, 156; (b) 2.94, 2.31, 127; (c) 3.08, 2.21, 162. 67
- Figure 2.17.** The sheet-like superstructure formed by the [2]pseudorotaxanes [5·7]⁺. The geometries of the π-π stacking interactions are (a) centroid-centroid distance 4.02 Å, rings inclined by 12°; (b) centroid-centroid distance 4.52 Å, mean interplanar separation 3.68 Å; (c) centroid-centroid distance 3.99 Å, mean interplanar separation 3.71 Å. The C-H···π interaction (d) is characterized by an H-π distance of 2.84 Å and a C-H···π angle of 140°. 68
- Figure 2.18.** (a) The crystal structure of BMP25C8 **5**. (b) Adjacent molecules are stacked by virtue of pairs of C-H···π interactions, (a) H···π distance 2.85 Å, C-H···π angle 140°; (b) H···π distance 2.79 Å, C-H···π angle 137°, supplemented by π-π stacking interactions between the resorcinol and catechol moieties, interactions *c* and *d*, respectively. (c) End-on view of the constricted nanotube formed by the stacking of BMP25C8 macrocycles. 69

Chapter 3: Supramolecular Daisy Chains

- Figure 3.1.** Top: A schematic representation of the covalent polymerization of monomer M^1 . 87
Bottom: A schematic representation of the noncovalent polymerization of a different monomer, M^2 .
- Figure 3.2.** The hydrogen-bond-mediated dimerization of 2-butylureido-6-methyl pyrimidone. 88
- Figure 3.3.** Reversible formation of a hydrogen-bonded linear supramolecular polymer formed 89
from a monomer bearing two 2-ureido-4-pyrimidone end groups.
- Figure 3.4.** A schematic representation depicting the formation of a threaded 1:1 complex (a 90
Pseudorotaxane) between two complementary species wherein the cavity of a suitably-sized *Ring*
is skewered by a linear *Rod*.
- Figure 3.5.** Conceptually, when two mutually-recognizing species are merged together, a single 90
self-complementary entity is formed.
- Figure 3.6.** A schematic representation depicting how a daisy chain monomer can self assemble 90
to form both cyclic and acyclic interwoven superstructures.
- Figure 3.7.** A schematic representation depicting the post-assembly kinetic capture—achieved 90
by ‘stoppering’ of the threaded portions of each monomer with a bulky end group over which the
macrocylic portions cannot pass—of an interwoven acyclic daisy chain.
- Figure 3.8.** Combining the features of both DB24C8 (**2**) and dibenzylammonium 91
hexafluorophosphate (**3**-H·PF₆) into one and the same molecule results in the design a self-
complementary daisy chain monomer **1**-H·PF₆.
- Figure 3.9.** The LSI-mass spectrum of **1**-H·PF₆. 92
- Figure 3.10.** (a) Ball-and-stick and (b) space-filling representations of the C₂ symmetric head-to- 94
tail dimer formed by **1**-H⁺.
- Figure 3.11.** The mosaic-like sheet of dimer pairs formed by **1**-H⁺. 94
- Figure 3.12.** The packing of dimers of **1**-H⁺, in one direction, *via* face-to-face π - π stacking 95
interactions and edge-to-face aromatic interactions.
- Figure 3.13.** The stacking of adjacent rows of dimers of **1**-H⁺, *via* C-H $\cdots\pi$ interactions. 95
- Figure 3.14.** The three cyclic stereoisomeric superstructures that can be formed upon dimerization 96
of **1**-H·PF₆.
- Figure 3.15.** The ¹H NMR spectra of **1**-H·PF₆ dissolved in (a) CD₃SOCD₃ (300 MHz, 298 K), 97
and (b) CD₃CN (400 MHz, 273 K).
- Figure 3.16.** An expansion of the two upfield-shifted aromatic doublets that appear in the ¹H 98
NMR spectrum (400 MHz, CD₃CN, 273 K) of **1**-H·PF₆.
- Figure 3.17.** ¹H NMR Spectra of (a) the amine **1**, followed by sequential addition of (b) 101
CF₃CO₂D (10 mol equiv) and (c) Et₃N (20 mol equiv).
- Figure 3.18.** The temperature-dependent (273-358 K) partial ¹H NMR spectra of a CD₃CN/D₂O 102
(98:2) solution of **1**-H·PF₆.

Figure 3.19. The concentration-dependent partial ^1H NMR spectra obtained from CD_3CN solutions of 1 -H·PF ₆ .	103
Figure 3.20. A schematic representation of the dynamic assembly of both acyclic and cyclic daisy chain superstructures (up to, and including, trimers) from a self-complementary monomer.	105
Figure 3.21. Concentration profiles—plotted using an Excel spreadsheet—that demonstrate how, based upon assumed K_a values, the concentration of daisy chain species in solution (expressed as a % of the total concentration of all species in solution) varies with the initial concentration of dissolved monomer (M).	106
Figure 3.22. The partial ^1H NMR spectrum (400 MHz, CDCl_3) of 13 , showing the residual peaks arising from the remaining H-resonances of the ‘catechol’ rings that were not 100 % deuterated.	109
Figure 3.23. The partial ^1H NMR spectrum (400 MHz, 300 K) of a CD_3CN solution of the deuterium-labeled daisy chain monomer 11 -H·PF ₆ . Two sets (\ddagger and \dagger) of signals are observed for the resonances of the protons (H_1 , H_2 , and H_3) of the central aromatic ring.	109
Figure 3.24. The chiral and achiral (<i>meso</i>) [c2]daisy chain superstructures that can be formed upon dimerization of a [24]crown-8 based monomer such as 11 -H·PF ₆ .	110
Figure 3.25. The partial ^1H NMR spectrum (400 MHz, 300 K) of a CD_3CN solution containing a 1:1 mixture of DB24C8 (2) and the <i>p</i> -F-substituted dibenzylammonium salt 14 -H·PF ₆ .	111
Figure 3.26. The partial ^{19}F NMR spectrum (376 MHz, 300 K) of a CD_3CN solution containing a 1:1 mixture of DB24C8 (2) and the <i>p</i> -F-substituted dibenzylammonium salt 14 -H·PF ₆ .	112
Figure 3.27. The partial ^{19}F NMR spectra (376 MHz, 300 K) of a 10 mM solution of 17 -H·PF ₆ dissolved in varying mixtures of $\text{CD}_3\text{CN}/\text{CD}_3\text{SOCD}_3$.	114
Figure 3.28. The partial ^1H NMR spectra (400 MHz, 300 K) of a 10 mM solution of 17 -H·PF ₆ dissolved in varying mixtures of $\text{CD}_3\text{CN}/\text{CD}_3\text{SOCD}_3$.	115
Figure 3.29. Partial ^1H NMR spectra (400 MHz, 300 K) recorded over time of a $\text{CDCl}_3/\text{CD}_3\text{CN}$ (3:1) solution containing a 1:1 mixture of DB24C8 (2) and the bis(3,5-difluoro)-substituted dibenzylammonium ion salt 18 -H·PF ₆ in a sealed NMR tube.	117
Figure 3.30. Partial ^{19}F NMR spectra (376 MHz, 300 K) recorded over time of a $\text{CDCl}_3/\text{CD}_3\text{CN}$ (3:1) solution containing a 1:1 mixture of DB24C8 (2) and the bis(3,5-difluoro)-substituted dibenzylammonium ion salt 18 -H·PF ₆ in a sealed NMR tube, reveal that the PF ₆ ⁻ anion decomposes in a matter of days under these conditions.	118
Figure 3.31. Surprisingly, the ^1H NMR spectrum (400 MHz, 300 K) of 21 -H·PF ₆ , obtained immediately after its dissolution in CD_3SOCD_3 , indicated the presence of aggregated daisy chain superstructures.	120
Figure 3.32. Partial ^{19}F NMR spectra (376 MHz, 300 K) recorded over time of a CD_3SOCD_3 solution of 21 -H·PF ₆ .	121
Figure 3.33. The FAB-mas spectra of 21 -H·PF ₆ (i) prior to dissolution in CD_3SOCD_3 , and (ii) after sitting in CD_3SOCD_3 solution for 6 d.	123

- Figure 3.34.** A schematic representation depicting the pathway *via* which a [c2]daisy chain superstructure is expected to disassemble to give, initially, the [a2]daisy chain, and then, ultimately, the monomeric species ([a1]daisy chain). 124
- Figure 3.35.** The FAB mass spectra of (i) an equimolar mixture of **1**-H·PF₆ {**H**} and **17**-H·PF₆ {**F**}, and (ii) an equimolar mixture of **17**-H·PF₆ {**F**} and **21**-H·PF₆ {**F**₂}. 125
- Figure 3.36.** The inherent symmetry of a [25]crown-8-based daisy chain monomer means that only one unique [c2]daisy chain can be formed upon aggregation. Similarly, only one [c3]-, one [c4]-, and one [c5]daisy chain, *etc...* can be formed. 126
- Figure 3.37.** The concentration-dependent partial ¹H NMR spectra (400 MHz, 300 K) of CD₂Cl₂ solutions of the parent [25]crown-8 daisy chain monomer (**22**-H·PF₆). 128
- Figure 3.38.** The partial ¹H NMR spectrum (400 MHz, 300 K) of a CD₃CN solution containing a 1:1 mixture of BMP25C8 (**28**) and the 3,5-difluorophenyl-substituted dibenzylammonium salt **18**-H·PF₆. 129
- Figure 3.39.** The partial ¹⁹F NMR spectrum (376 MHz, 300 K) of a 1:1 mixture of BMP25C8 (**28**) and **18**-H·PF₆ reveals the presence of two aromatic F signals, one corresponding to free **18**-H·PF₆, and the other to the [2]pseudorotaxane [**28**·**18**-H]PF₆. 130
- Figure 3.40.** The concentration-dependent partial ¹⁹F NMR spectra (376 MHz, 298 K, CD₃CN) of **29**-H·PF₆. 131
- Figure 3.41.** A schematic representation depicting the ‘free’ and bound ammonium ion-containing arms of aggregated (up to, and including, trimeric) daisy chain superstructures. 132
- Figure 3.42.** The expressions used to calculate the association constants for the aggregation of **29**-H·PF₆ in CD₃CN solution at 298 K. 133
- Figure 3.43.** A concentration profile can be constructed for **29**-H·PF₆ based upon the *K_a* values determined from the ¹⁹F NMR spectroscopic studies. 134
- Figure 3.44.** Expressions for the overall cyclic dimerization and trimerization constants in a self-complementary daisy chain system. 135
- Figure 3.45.** The temperature-dependent partial ¹⁹F NMR spectra (376 MHz, CD₃CN) of **29**-H·PF₆. 136
- Figure 3.46.** The van’t Hoff plot obtained upon plotting ln *K_a* vs 1/*T* for the *K_a* values determined from the partial ¹⁹F NMR spectra illustrated in Figure 3.45. 137
- Figure 3.47.** A schematic representation depicting the possible ways in which a bidirectional quadratropic daisy chain monomer may self-assemble to form aggregated superstructures. 139
- Figure 3.48.** A schematic representation depicting the covalent polymerization of a discrete [c2]daisy chain superstructure to afford an interlocked macromolecule. 140

Chapter 4: Kinetic and Thermodynamic Approaches for the Synthesis of Ammonium Ion/Crown Ether-Based Interlocked Molecules

- Figure 4.1.** A schematic representation of the generic structures of the two most widely studied classes of interlocked molecules. 165
- Figure 4.2.** A schematic representation depicting the kinetic synthesis of a [2]catenane from the appropriate [2]pseudorotaxane. 167
- Figure 4.3.** Both (a) stoppering, and (b) clipping approaches can be utilized for the synthesis—performed under kinetic control—of a [2]rotaxane. 167
- Figure 4.4.** The slippage synthesis of a ‘rotaxane-like’ complex relies upon the precise matching of the end groups of the dumbbell and the size of the cavity of the macrocyclic through which the dumbbell has to pass. 168
- Figure 4.5.** A schematic representation depicting the thermodynamically-controlled synthesis of a [2]rotaxane using the ‘stoppering’ methodology. Note: the thinner lines represent the reversibly-formed covalent bonds; a convention that will be used throughout the remainder of this Chapter. 169
- Figure 4.6.** A schematic representation depicting the thermodynamically-controlled synthesis of a dynamic [2]rotaxane utilizing ‘clipping’ methodology. 170
- Figure 4.7.** Schematic representations of dynamic interlocked structures (catenanes **I-II** and rotaxanes **III-V**) which differ in the location of the reversible covalent bonds. For example, whereas the dumbbell of **III** can be formed and broken reversibly, it is the ring component of **IV** that contains the reversible covalent bonds. Consequently, dynamic rotaxane **III** would be formed by a ‘stoppering’ approach, whereas **IV** would require a clipping strategy. Rotaxane **V**, in which both components contain reversibly-formed linkages, could be assembled *via* either pathway. 170
- Figure 4.8.** Schematic representations of ‘magic’ interlocked molecules! 171
- Figure 4.9.** Conceptually, the assembly of an amino-functionalized [2]semirotaxane and subsequent reaction with a bulky isocyanate leads to the formation of a ureido-[2]rotaxane. 172
- Figure 4.10.** The structure of the [2]rotaxane **1-H·O₂CCF₃**, showing the labeling scheme for both (i) the dumbbell and (ii) the crown ether components, used in describing its NMR spectroscopic properties. The schematic representation (ii) highlights the unsymmetrical nature of the dumbbell. The protons (α^1 , β^1 , γ^1) on one face of the DB24C8 macrocycle are oriented toward the 3,5-di-*tert*-butylphenyl stopper, whereas those protons (α^2 , β^2 , γ^2) on the opposite face of the macrocycle are directed toward the 2,6-diisopropylphenyl stopper, *i.e.*, the protons located on opposite faces of the crown ether are diastereotopic. 174
- Figure 4.11.** The partial ¹H NMR spectrum (400 MHz, CD₂Cl₂) of **1-H·O₂CCF₃**. 175
- Figure 4.12.** The partial T-ROESY spectrum (400 MHz, CD₂Cl₂) of **1-H·O₂CCF₃**. The most significant probe protons are H-2 and H-3, which each show a correlation to only one set of protons on only one face of the crown ether. 176

Figure 4.13 The molecular structures of the two crystallographically-independent [2]rotaxanes present in the crystals of **1**-H·O₂CCF₃. Hydrogen bonding distances and angles {[X···O], [H···O] distances (Å), [X–H···O] angles (°)}: for molecule **(i)**; **(a)** 2.85, 2.01, 156; **(b)** 2.89, 2.16, 137; **(c)** 3.31, 2.36, 171; **(e)** 2.89, 2.03, 159; **(f)** 2.86, 1.98, 164; for molecule **(ii)**; **(a)** 2.91, 2.11, 147; **(b)** 3.01, 2.23, 145; **(c)** 3.41, 2.51, 157; **(d)** 3.25, 2.41, 147; **(e)** 2.76, 1.92, 163; **(f)** 2.91, 2.02, 168. The centroid-centroid distances **(g)** for molecules **(i)** and **(ii)** are 4.48 and 4.54 Å, respectively. 177

Figure 4.14. The partial ¹H NMR spectrum (400 MHz, CD₂Cl₂) of **7**-H·O₂CCF₃. Note (*) that the broad peak at δ = 9.4 ppm is a background signal arising from the NMR probe. 179

Figure 4.15. The structure of the [2]rotaxane **7**-H·O₂CCF₃, showing the labeling scheme for the protons on both **(i)** the dumbbell and **(ii)** the crown ether components, used in describing its NMR spectroscopic parameters. The through-space correlations determined by T-ROESY measurements are also highlighted in **(i)** by double-headed arrows. The schematic representation **(ii)** highlights the unsymmetrical nature of the dumbbell. The protons (α¹, β¹, γ¹, δ¹, ε¹, φ¹) on one face of the BMP25C8 macrocycle are oriented toward the 3,5-di-*tert*-butylphenyl stopper, whereas those protons (α², β², γ², δ², ε², φ²) on the opposite face of the macrocycle are directed toward the 2,6-diisopropylphenyl stopper. 180

Figure 4.16. Partial ¹³C NMR spectra (125 MHz, CD₃CN:CD₃SOCD₃ 3:1), recorded at various temperatures, showing the coalescence of the signal arising from the carbon atom of the methyl groups that constitute the isopropyl groups. 181

Figure 4.17. A Ramachandran-like plot depicting the energy profile of bond rotations associated with the 2,6-diisopropylphenyl stopper moiety. 182

Figure 4.18. The molecular structures of the two crystallographically-independent [2]rotaxanes present in the crystals of **7**-H·O₂CCF₃. Hydrogen bonding distances and angles {[X···O], [H···O] distances (Å), [X–H···O] angles (°)}: for molecule **(i)**; **(a)** 2.90, 2.07, 152; **(b)** 2.92, 2.17, 140; **(c)** 3.06, 2.26, 149; **(d)** 3.34, 2.48, 149; **(e)** 2.83, 1.95, 163; **(f)** 2.88, 2.00, 166; for molecule **(ii)**; **(a)** 2.83, 1.94, 170; **(b)** 2.95, 2.34, 125; **(c)** 3.13, 2.26, 163; **(d*)** 3.30, 2.43, 150; **(e)** 2.93, 2.04, 170; **(f)** 2.89, 2.00, 172; **(g)** 3.22, 2.42, 141. The centroid-centroid distances **(h)** for molecules **(i)** and **(ii)** are 4.22 and 4.29 Å, respectively. 183

Figure 4.19. Signals for the resonances corresponding to (i) free crown ether **5** (ii) uncomplexed thread **9**-H·PF₆ and (iii) the 1:1 pseudorotaxane complex [**5**·**9**-H]PF₆ formed between the two individual components can be observed in the ¹H NMR spectrum. This phenomenon indicates that the free and complexed species are equilibrating slowly on the NMR timescale and therefore allows for the simple calculation of K_a by utilizing the so-called single-point method. 186

Figure 4.20. Left: Partial ¹H NMR spectra (400 MHz, CD₃CN, 300 K), recorded over time, of an initial mixture of dialdehyde **9**-H·PF₆ (20 mM) and 3,5-di-*tert*-butylaniline **12** (40 mM). Right: The dynamic equilibrium established in solution, and the corresponding percentages of 187

each of the three species at equilibrium. The probe protons of, and the associated resonances for, the dialdehyde are labeled '9' (*i.e.*, corresponding to compound 9-H·PF₆), those of the monoaldehyde (monoimine) '13', and those of the diimine dumbbell '14'.

Figure 4.21. Top: A schematic representation of the dynamic process under spectroscopic investigation. Bottom: The partial ¹H NMR spectrum (400 MHz, CD₃CN, 300 K), recorded over time, of an initial mixture of 9-H·PF₆ (20 mM), 3,5-di-*tert*-butyl-aniline **12** (40 mM), which was allowed to reach equilibrium (spectrum at *t* = 0 min) prior to the addition of DB24C8 (**5**) (20 mM). Peaks corresponding to species containing an NH₂⁺ center not bound/occupied by a DB24C8 ring are colored black, while those which correspond to species that are bound/occupied are shaded grey and, furthermore, the numerical labels attached to these peaks are suffixed with an asterisk. The signals associated with the dialdehyde {9}, monoaldehyde {13} and diimine {14} probe protons are highlighted as described in Figure 4.20. 188

Figure 4.22. Top: A schematic representation of the dynamic process under spectroscopic investigation. Bottom: The partial ¹H NMR spectrum (400 MHz, CD₃CN, 300 K) recorded over time, of an initial mixture of 9-H·PF₆ (20 mM), 3,5-di-*t*-butylaniline **12** (40 mM) and DB24C8 (**5**) (20 mM). Peaks are annotated in the same fashion as in Figure 4.21. 189

Figure 4.23. A schematic representation demonstrating the principle of thermodynamically-driven rotaxane synthesis *via* an imine exchange (rather than imine formation/hydrolysis) pathway. 192

Figure 4.24. The reaction of the dialdehyde compound (9-H·PF₆) with a difunctional aniline (*e.g.*, *m*-phenylenediamine **17**) can yield two types of product. At lower concentrations, the formation of catenanes is anticipated, however, upon increasing the concentration, linear pseudopolyrotaxanes may be formed. 193

LIST OF SCHEMES

Chapter 2: The Influence of Macrocyclic Polyether Constitution upon Ammonium Ion Binding

Scheme 2.1. The synthesis of BMP25C8 (**5**). 52

Chapter 3: Supramolecular Daisy Chains

Scheme 3.1. The synthesis of the parent [24]crown-8 daisy chain monomer **1**-H·PF₆. 92

Scheme 3.2. The synthesis of catechol-*d*₄ (**12**) from catechol (**8**). 108

Scheme 3.3. The synthesis of the deuterium-labeled daisy chain monomer **11**-H·PF₆. 108

Scheme 3.4. The synthesis of bis(4-fluorobenzyl)ammonium hexafluorophosphate (14 -H·PF ₆).	111
Scheme 3.5. The synthesis of a <i>p</i> -F-substituted daisy chain monomer 17 -H·PF ₆ .	113
Scheme 3.6. The synthesis of bis(3,5-difluorobenzyl)ammonium hexafluorophosphate (18 -H·PF ₆).	116
Scheme 3.7. The synthesis of the 3,5-difluorophenyl-terminated [24]crown-8 daisy chain monomer 21 -H·PF ₆ .	119
Scheme 3.8. The synthesis of the parent [25]crown-8-based daisy chain monomer 22 -H·PF ₆ .	127
Scheme 3.9. The synthesis of the 3,5-difluorophenyl-terminated [25]crown-8 daisy chain monomer.	131

Chapter 4: Kinetic and Thermodynamic Approaches for the Synthesis of Ammonium Ion/Crown Ether-Based Interlocked Molecules

Scheme 4.1. The synthesis of the [2]rotaxane 1 -H·O ₂ CCF ₃ .	173
Scheme 4.2. The synthesis of the first BMP25C8-containing [2]rotaxane 7 -H·O ₂ CCF ₃ .	178
Scheme 4.3. Synthesis of the dialdehyde 9 -H·PF ₆ .	185
Scheme 4.4. The dynamic equilibrium established upon dissolution of a 1:2:1 ratio (20:40:20 mM) of 9 -H·PF ₆ , 3,5-di- <i>tert</i> -butylaniline (12) and DB24C8 (5) in CD ₃ CN.	190
Scheme 4.5. 'Fixing' of the dynamic system upon reduction with PhSeH, thus affording the kinetically-stable [2]rotaxane 15 -H·PF ₆ .	191

LIST OF TABLES

Chapter 2: The Influence of Macrocyclic Polyether Constitution upon Ammonium Ion Binding

Table 2.1. Relative intensities of complexed and uncomplexed species in the 'gas phase' as determined by LSIMS.	53
Table 2.2. The stability constants (K_a 's) calculated for the formation of pseudorotaxanes incorporating crown ethers 1-3 , 5 and 6 with guests 7-9 ·PF ₆ .	55
Table 2.3. [N ⁺ -H···O] and [C-H···O] hydrogen bonding parameters <i>a-d</i> and centroid-centroid separations (Å) for pairs of aromatic rings in the four independent [TB24C8· 7]PF ₆ supermolecules (Figure 2.8) that exist in the solid state.	62
Table 2.4. Hydrogen bond lengths (Å) for the interactions between the F atoms of the PF ₆ ⁻ anions and the H atoms located on either the 7 ⁺ cation or the TB24C8 ring in the four independent [TB24C8· 7]PF ₆ supermolecules that exist in the solid state.	63

Chapter 4: Kinetic and Thermodynamic Approaches for the Synthesis of Ammonium Ion/Crown Ether-Based Interlocked Molecules

Table 4.1. The torsion angles (**w**, **x**, **y** and **z**) observed for the DB24C8- and BMP25C8-containing rotaxanes, **1**-H·O₂CCF₃ and **7**-H·O₂CCF₃, respectively. In each structure, there are two crystallographically-independent molecules (**i** and **ii**) in the asymmetric unit. 177

LIST OF SYMBOLS AND ABBREVIATIONS

24C8	[24]Crown-8
Å	Ångstroms
B24C8	Benzo[24]crown-8
BMP25C8	Benzometaphenylene[25]crown-8
BPP34C10	Bisparaphenylene[34]crown-10
COSY	Correlation Spectroscopy
DBA	Dibenzylammonium
DMAP	4-Dimethylaminopyridine
DMF	<i>N,N</i> -Dimethylformamide
DMSO	Dimethylsulfoxide
DP	Degree of Polymerization
EIMS	Electron Impact Mass Spectrometry
Et ₂ O	Diethyl Ether
Et ₃ N	Triethylamine
EtOAc	Ethyl Acetate
EPR	Electron Paramagnetic Resonance
FABMS	Fast Atom Bombardment Mass Spectrometry
GC	Gas Chromatography
HMQC	Heteronuclear Multiple Quantum Correlation
HRMS	High Resolution Mass Spectrometry
<i>K</i> _a	Association Constant
kcal	Kilocalories
kJ	Kilojoules
LSIMS	Liquid Secondary Ion Mass Spectrometry
Me ₂ CO	Acetone
MeCN	Acetonitrile
MeNO ₂	Nitromethane

MeOH	Methanol
MHz	Megahertz
mM	Millimolar
<i>m/z</i>	Mass-to-charge ratio
NMR	Nuclear Magnetic Resonance
PCC	Pyridinium Chlorochromate
PhMe	Toluene
PhSeH	Benzeneselenol
ppm	Parts per million
TB24C8	Tetrabenzocrown-8
TB27C9	Tribenzocrown-9
THF	Tetrahydrofuran
TPP51C15	Trisparaphenylene[51]crown-15
TPP68C20	Tetrakisparaphenylene[68]crown-20
T-ROESY	Transverse Rotating-Frame Overhauser Enhancement Spectroscopy
TsCl	4-Toluenesulfonyl Chloride

Note: When a standard chemical formula (*i.e.*, one containing symbols only representing chemical elements and not functional group abbreviations) is used to describe a compound in this Thesis, the formula is not reproduced in the table above.

ACKNOWLEDGEMENTS

The research reported in this Thesis not only spans just over four and a half years, but also two continents. This journey began at the University of Birmingham in the UK, and now draws to a close some 5000 or so miles distant, at the University of California, Los Angeles. Therefore, not only has working in Fraser's group been a thoroughly enjoyable experience, but it has given me the opportunity to see much more of the world than I ever thought I would! I feel very privileged to have been a part of the Stoddart group, and to have known some of the people who have shared the experience with me. Therefore, whereas the words and pictures on the pages of this Thesis tell the story of the science that has interested, intrigued, frustrated, and occasionally amused me over the past few years, this small—but significant—section features the people who have made it all possible.

I am deeply indebted to Fraser for welcoming me into his research group, for providing me with great facilities, for his advice and encouragement, and for all the opportunities I have had to travel far and wide to tell the world about the chemistry I have done. More than that, however, thanks for supporting me through some life-changing decisions, for listening when I really needed you to listen, and for going out of your way to help me on numerous occasions. I also wish to thank Norma Stoddart, who has played a major role in keeping me sane over the past few months, offering me valuable pieces of advice from across the office as I have sat staring blankly at a computer screen trying to compose this Thesis. Indeed, Norma's wicked sense of humour has rescued me on more than one occasion. Furthermore, if I manage to live out the rest of my life with only one tenth of the strength, courage, and bravery, of such a remarkable lady, then I will be fine. Thank you both very, very much.

I remember fondly my days at the University of Birmingham, and I wish to thank the following people who were there with me: Jürgen Huff, Sue Boyd, Chris Brown, Giuseppe Gattuso, Andy Robertson, Andy Shipway, Simon Newton, Olda Kocian, Justine Walter, Vikki Allen, Ceri Booth, Simon Everitt, Wayne Hayes, Dario Pasini, Masumi Asakawa, Christian Claessens, Christoph Hamers, Reinhard Wolf, Marcos Gómez-López, Doug Philp, and Jon Preece.

I am grateful to Peter Glink for getting me started on the daisy chain project, and for his constant advice during the course of my PhD studies. He has also taken much time to expertly proof-read many of my manuscripts, including the first half of this Thesis.

During my time at Birmingham, and on subsequent return visits since, I have enjoyed immensely the discussions I have had with Ian Parsons. I thank him for welcoming me into his office, plying me with coffee, and listening with enthusiasm as I talk about my results and ideas. His advice and suggestions have spurred me on, and my PhD studies are better for it.

I am very grateful to Owen Matthews for his supervision throughout the first year of my PhD studies in Birmingham. During that time I gained a very good friend who has guided me since. Owen has been a constant source of invaluable advice, and when there's a difficult decision to make, he's one of the first people I turn to. And even though I don't always follow his suggestions, deep down I know that I probably should!

I wish to thank Aaron Heiss for his advice, support, and friendship over the past four years. He always knows when to drag me out for a beer and how to make the world seem not so bad. His constant reassurance made the move to the United States less traumatic, and he—along with his wife Anne—have gone out of their way to make it feel like home since.

I owe a great deal of thanks to Neil Spencer at the University of Birmingham, who has given so much of his time and expertise in pursuit of solutions to my many NMR spectroscopic conundrums. At UCLA, that challenge was taken up by Jane Strouse, whom I thank for her valuable advice and suggestions. Until someone can convince me otherwise, the greatest mass spectrometrist in the world is Pete Ashton at the University of Birmingham. Always willing to help, no problem is too big or too small for Pete, and he continues to run the occasional sample that I ship back to England. Thank you.

I have had the good fortune to make two trips to Imperial College, London, to spend time with Professor David Williams. On the first occasion, he and his group performed a rather swift X-ray crystallographic analysis for me when I arrived from Birmingham—practically unannounced—clutching my precious crystals, grown only the day before. Later, when I flew home from the US for the Christmas break in 1998, I spent three days of the following New Year visiting his laboratories. Each time, I was made to feel very welcome, and I thank him and his group for their time and hospitality, in addition to the expert X-ray crystallographic analyses they have performed.

Thanks also to Natalie Rowley, Melanie Coles, and Helen Vahey, for always welcoming me back to the School of Chemistry at Birmingham with coffee, biscuits, and gossip. I am also

grateful to Natalie for the chance to collaborate with her on some porphyrin-based systems that, unfortunately, did not make it into this Thesis. On my visits back to Birmingham—as well as *via* e-mail—I am grateful for the interest Natalie always shows in my work, in addition to the encouragement she offers.

I also wish to thank Gunter Mattersteig, Matthew Fyfe, Theresa Chang, Gilmer Youn, Bruce Turnbull, Ludek Ridvan, Sheng-Hsien Chiu, Arkadij Elizarov, Matthias Horn, Jan Jeppesen, Dafni Amirsakis, Jiangao Cao, Al Nelson, Sebastien Vidal, and Julie Perkins, for their friendship during my time at UCLA. I also thank Glenn Norohna for the many scientific and philosophical discussions we have engaged in. Furthermore, I really enjoyed the opportunity to be a teaching assistant for two of the classes Glenn taught at UCLA.

Upon my arrival at UCLA, Jake Wasserman made everything happen. From the Federal Building to furniture buying, Jake helped with every aspect of settling into LA life. Indeed, the Stoddart group as a whole owes a great debt of gratitude to Jake for the vast amount of work he put into making sure that we were all looked after.

I started my PhD studies at the same time as four others, Sarah Hickingbottom, James Lowe, David Fulton, and Anthony Pease. We have all followed the same path—from Birmingham to UCLA—and I thank each one of them for their friendship and support along the way.

I wish to thank Stuart Rowan both for his sound scientific advice and his friendship. I have learned a lot from him, and the research contained within this Thesis has benefited from the many hours of discussions we have shared.

I am grateful to Sabine Wenger for her thoughtful advice—with regard to both chemistry *and* life—and I treasure the friendship we have.

Finally, without the love and support of my family, none of this would have been possible. Thank you all. And to Maggie, thank you for everything – I love you.

The research reported in this Thesis was performed under the supervision of Professor J Fraser Stoddart. Initially (1996–1997), the work was carried out in the School of Chemistry at the University of Birmingham (UK), and then subsequently (1997–2001) in the Department of Chemistry and Biochemistry at the University of California, Los Angeles

(USA). Funding was provided by the Engineering and Physical Sciences Research Council in the UK, and by the University of California, Los Angeles in the USA.

Chapter 1 of this Thesis is based on the following Review article: Cantrill, S. J.; Pease A. R.; Stoddart, J. F. *J. Chem. Soc., Dalton Trans.* **2000**, 3715–3734. The many talented graduate students and postdoctoral researchers who have contributed to the creation of the molecular meccano kit described in this Chapter are acknowledged. Professor David J Williams and Dr Andrew J P White at Imperial College, London, are thanked for all of the X-ray crystallographic studies performed on the superstructures described therein.

Chapter 2 of this Thesis is based on the following publications: (1) Ashton, P. R.; Bartsch, R. A.; Cantrill, S. J.; Hanes, Jr., R. E.; Hickingbottom, S. K.; Lowe, J. N.; Preece, J. A.; Stoddart, J. F.; Talanov, V. S.; Wang, Z.-H. *Tetrahedron Lett.* **1999**, *40*, 3661–3664. (2) Ashton, P. R.; Cantrill, S. J.; Preece, J. A.; Stoddart, J. F.; Wang, Z.-H.; White, A. J. P.; Williams, D. J. *Org. Lett.* **1999**, *1*, 1917–1920. (3) Cantrill, S. J.; Fulton, D. A.; Heiss, A. M.; Pease, A. R.; Stoddart, J. F.; White, A. J. P.; Williams, D. J. *Chem. Eur. J.* **2000**, *6*, 2274–2287. (4) Cantrill, S. J.; Preece, J. A.; Stoddart, J. F.; Wang, Z.-H.; White, A. J. P.; Williams, D. J. *Tetrahedron* **2000**, *56*, 6675–6681.

Chapter 3 of this Thesis is based on the following publications: (1) Ashton, P. R.; Baxter, I.; Cantrill, S. J.; Fyfe, M. C. T.; Glink, P. T.; Stoddart, J. F.; White, A. J. P.; Williams, D. J. *Angew. Chem., Int. Ed.* **1998**, *37*, 1294–1297. (2) Cantrill, S. J.; Stoddart, J. F.; Williams, D. J. *Am. Chem. Soc., Polym. Prepr.* **1999**, *40(2)*, 1130–1131.

Chapter 4 of this Thesis is based on the following publications: (1) Cantrill, S. J.; Fulton, D. A.; Fyfe, M. C. T.; Stoddart, J. F.; White, A. J. P.; Williams, D. J. *Tetrahedron Lett.* **1999**, *40*, 3669–3672. (2) Cantrill, S. J.; Rowan, S. J.; Stoddart, J. F. *Org. Lett.* **1999**, *1*, 1363–1366. (3) Cantrill, S. J.; Fulton, D. A.; Heiss, A. M.; Pease, A. R.; Stoddart, J. F.; White, A. J. P.; Williams, D. J. *Chem. Eur. J.* **2000**, *6*, 2274–2287.

VITA

- April 12, 1974 Born, Lichfield, England
- 1995 Frankland Prize for Excellence in Practical Chemistry
University of Birmingham
Edgbaston, Birmingham, England
- 1996 BSc (Hons) First Class, Chemistry & Bioorganic Chemistry
University of Birmingham
Edgbaston, Birmingham, England
- 1997 MPhil (Sci), Chemistry
University of Birmingham
Edgbaston, Birmingham, England
- 1999 Cram Research Award
University of California, Los Angeles
Los Angeles, California, USA
- 2000 Winstein Dissertation Award
University of California, Los Angeles
Los Angeles, California, USA

PUBLICATIONS AND PRESENTATIONS

Poster Presentation: **Cantrill, S. J.**; Fyfe, M. C. T.; Glink, P. T.; Schiavo, C.; Stoddart, J. F., “The Self-Assembly of Pseudorotaxanes and Rotaxanes formed between Secondary Dialkylammonium Salts and Crown Ethers”, Crystal Engineering, NATO ASI Meeting, Digby, Nova Scotia, Canada, Sept 13–25th, 1996.

Ashton, P. R.; **Cantrill, S. J.**; Gattuso, G.; Menzer, S.; Nepogodiev, S. A.; Shipway, A. N.; Stoddart, J. F.; Williams, D. J., “Achiral Cyclodextrin Analogues”, *Chem. Eur. J.* **1997**, *3*, 1299–1314.

Ashton, P. R.; Baxter, I.; **Cantrill, S. J.**; Fyfe, M. C. T.; Glink, P. T.; Stoddart, J. F.; White, A. J. P.; Williams, D. J., "Supramolecular Daisy Chains", *Angew. Chem., Int. Ed.* **1998**, *37*, 1294–1297.

Cantrill, S. J.; Fyfe, M. C. T.; Raymo, F. M.; Stoddart, J. F.; "Synthetic Supramolecular Chemistry", In *Current Challenges on Large Supramolecular Assemblies*; Tsoucaris, G., Ed.; Kluwer: Dordrecht, 1998; pp. 17–35.

Poster Presentation: Ashton, P. R.; Baxter, I.; **Cantrill, S. J.**; Fyfe, M. C. T.; Glink, P. T.; Stoddart, J. F.; White, A. J. P.; Williams, D. J., "Supramolecular Daisy Chains", *Macrocycles in Academe and Industry, XXIII International Symposium on Macrocyclic Chemistry*, Hawaii, USA, June 7–12th, 1998.

Poster Presentation: **Cantrill, S. J.**; Rowan, S. J.; Stoddart, J. F., "Kinetic and Thermodynamic Approaches to the Syntheses of Interlocked Molecules", *Supramolecular Science, NATO ARW Meeting, Lerici, Italy*, Sept 4–7th, 1998.

Cantrill, S. J.; Fyfe, M. C. T.; Raymo, F. M.; Stoddart, J. F.; "Probing Self-Assembly by NMR", In *Applications of NMR to the Study of Structure and Dynamics of Supramolecular Complexes*; Pons, M., Ed.; Kluwer: Dordrecht, 1999; pp. 1–18.

Ashton, P. R.; Bartsch, R. A.; **Cantrill, S. J.**; Hanes, Jr., R. E.; Hickingbottom, S. K.; Lowe, J. N.; Preece, J. A.; Stoddart, J. F.; Talanov, V. S.; Wang, Z.-H., "Secondary Dibenzylammonium Ion Binding by [24]Crown-8 and [25]Crown-8 Macrocycles", *Tetrahedron Lett.* **1999**, *40*, 3661–3664.

Cantrill, S. J.; Fulton, D. A.; Fyfe, M. C. T.; Stoddart, J. F.; White, A. J. P.; Williams, D. J., "A New Protocol for Rotaxane Synthesis", *Tetrahedron Lett.* **1999**, *40*, 3669–3672.

Rowan, S. J.; **Cantrill, S. J.**; Stoddart, J. F., "Triphenylphosphonium-Stoppered [2]Rotaxanes", *Org. Lett.* **1999**, *1*, 129–132.

Cantrill, S. J.; Fyfe, M. C. T.; Heiss, A. M.; Stoddart, J. F.; White, A. J. P.; Williams, D. J., "Rotaxane Construction with a Binaphthol-Derived Crown Ether", *Chem. Commun.* **1999**, 1251–1252.

Rowan, S. J.; **Cantrill, S. J.**; Stoddart, J. F., "Wittig Reactions on Phosphonium-Stoppered [2]Rotaxanes. A New Route to Macromolecular Daisy Chains?", *Am. Chem. Soc., Polym. Prepr.* **1999**, *40(2)*, 1119–1120.

Cantrill, S. J.; Stoddart, J. F.; Williams, D. J., “Supramolecular Daisy Chains”, *Am. Chem. Soc., Polym. Prepr.* **1999**, *40*(2), 1130–1131.

Poster Presentation: **Cantrill, S. J.**; Stoddart, J. F.; Williams, D. J., “(Supra)molecular Daisy Chains”, Polymer Division, 218th ACS National Meeting, New Orleans, USA, Aug 22–26th, 1999.

Oral Presentation: **Cantrill, S. J.**; Stoddart, J. F.; Rowan, S. J., “Rotaxane Formation Under Thermodynamic Control”, Organic Division, 218th ACS National Meeting, New Orleans, USA, Aug 22–26th, 1999.

Cantrill, S. J.; Rowan, S. J.; Stoddart, J. F., “Rotaxane Formation Under Thermodynamic Control”, *Org. Lett.* **1999**, *1*, 1363–1366.

Ashton, P. R.; **Cantrill, S. J.**; Preece, J. A.; Stoddart, J. F.; Wang, Z.-H.; White, A. J. P.; Williams, D. J., “Anion-Orchestrated Formation in the Crystalline State of [2]Pseudorotaxane Arrays”, *Org. Lett.* **1999**, *1*, 1917–1920.

Cantrill, S. J., “Ammonia”, In *World of Chemistry*; Young, R. V.; Sessine, S., Eds.; Gale Group, 1999; pp. 44.

Cantrill, S. J.; Fyfe, M. C. T.; Heiss, A. M.; Stoddart, J. F.; White, A. J. P.; Williams, D. J., “Tribenzo[27]crown-9: A New Ring for Dibenzylammonium Rods”, *Org. Lett.* **2000**, *2*, 61–64.

Oral Presentation: **Cantrill, S. J.**; Stoddart, J. F.; Rowan, S. J., “Rotaxane Formation Under Thermodynamic Control”, NAIR Workshop on Chemo-Intelligence, Tsukuba, Japan, Mar 7th, 2000.

Rowan, S. J.; **Cantrill, S. J.**; Stoddart, J. F.; White, A. J. P.; Williams, D. J., “Toward Daisy Chain Polymers: ‘Wittig Exchange’ of Stoppers in [2]Rotaxane Monomers”, *Org. Lett.* **2000**, *2*, 759–762.

Poster Presentation: **Cantrill, S. J.**; Stoddart, J. F.; Williams, D. J., “(Supra)molecular Daisy Chains”, Macrocycles 2000, XXV International Symposium on Macrocyclic Chemistry, St Andrews, Scotland, July 2–7th, 2000.

Poster Presentation: **Cantrill, S. J.**; Stoddart, J. F.; Youn, G. J., “Studies on the Self Assembly of Supramolecular Daisy Chain Architectures”, ISSC 2000, XI International Symposium on Supramolecular Chemistry, Fukuoka, Japan, July 30–Aug 4th, 2000.

Cantrill, S. J.; Fulton, D. A.; Heiss, A. M.; Pease, A. R.; Stoddart, J. F.; White, A. J. P.; Williams, D. J., “The Influence of Macrocyclic Polyether Constitution upon Ammonium Ion/Crown Ether Recognition Processes”, *Chem. Eur. J.* **2000**, *6*, 2274–2287.

Cantrill, S. J.; Preece, J. A.; Stoddart, J. F.; Wang, Z.-H.; White, A. J. P.; Williams, D. J., “The Idiosyncrasies of Tetrabenzo[24]crown-8 in the Solid State”, *Tetrahedron* **2000**, *56*, 6675–6681.

Chang, T.; Heiss, A. M.; **Cantrill, S. J.**; Fyfe, M. C. T.; Pease, A. R.; Rowan, S. J.; Stoddart, J. F.; Williams, D. J., “Toward Interlocked Molecules Beyond Catenanes and Rotaxanes”, *Org. Lett.* **2000**, *2*, 2943–2946.

Chang, T.; Heiss, A. M.; **Cantrill, S. J.**; Fyfe, M. C. T.; Pease, A. R.; Rowan, S. J.; Stoddart, J. F.; White, A. J. P.; Williams, D. J., “Ammonium Ion Binding with Pyridine-Containing Crown Ethers”, *Org. Lett.* **2000**, *2*, 2947–2950.

Chiu, S.-H.; Rowan, S. J.; **Cantrill, S. J.**; Glink, P. T.; Garrell, R. L.; Stoddart, J. F., “A Rotaxane-Like Complex with Controlled-Release Characteristics”, *Org. Lett.* **2000**, *2*, 3631–3634.

Cantrill, S. J.; Pease A. R.; Stoddart, J. F., “A Molecular Meccano Kit”, *J. Chem. Soc., Dalton Trans.* **2000**, 3715–3734.

ABSTRACT OF THE DISSERTATION

Some Adventures in
Secondary Ammonium Ion
Binding

by

Stuart James Cantrill

Doctor of Philosophy in Chemistry

University of California, Los Angeles, 2001

Professor J Fraser Stoddart, Chair

A range of secondary ammonium ($R_2NH_2^+$) ions have been shown to thread through the cavities of appropriately-sized crown ethers to afford interwoven complexes. X-Ray crystallographic investigations to probe the solid-state properties of these supermolecules have revealed (*Chapter 1*) that many subtle factors—*e.g.*, solvents of crystallization, crown ether conformations and anion interactions—can influence the nature of the overall three-dimensional superstructures. Furthermore, a comparison of differently-substituted crown ethers—possessing either [24]crown-8 or [25]crown-8 constitutions—has revealed (*Chapter 2*) that relatively small mutations in the structure of the macrocyclic polyether

can have profound consequences upon its ability to bind $R_2NH_2^+$ ions. Substitution of the [24]crown-8 framework with increasing numbers of benzo rings is observed to lower the stability constants (K_a 's) from $>10^3$ to $\sim 0 M^{-1}$ in acetonitrile, and a pronounced decrease in K_a values also occurs when the [24]crown-8 constitution is expanded to give a macroring containing 25 atoms. Building upon the results obtained for these simple binary systems, self-complementary daisy chain monomers—in which a secondary ammonium ion-containing arm is grafted onto a macrocycle with either a [24]- or [25]crown-8 constitution—were synthesized, and shown (*Chapter 3*) to form small aggregates in the 'gas', solution, and solid phases. Finally, both kinetic and thermodynamic approaches have been employed (*Chapter 4*) in the synthesis of rotaxanes based upon the secondary ammonium ion/crown ether recognition site. The reaction between amino and isocyanate groups has been exploited for the synthesis—under kinetic control—of both DB24C8- and BMP25C8-containing ureido-[2]rotaxanes, the latter of which represents the first example of an interlocked structure incorporating this particular crown ether. Conversely, a thermodynamically-control synthesis is achieved when DB24C8 is added to a solution containing a diimine dumbbell-like component, wherein the dynamic nature of the system (*i.e.*, imine hydrolysis/reformation) offers the ring component access to the NH_2^+ center, allowing the self-assembly of the corresponding 'dynamic' [2]rotaxane to occur. Furthermore, the 'fixing' of this [2]rotaxane can be achieved upon reduction of the imine bonds, affording a kinetically-inert [2]rotaxane.